metals

MDPI

Article

Study on the Mechanical and Tribological Properties and the Mechanisms of Cr-Free Ni-Based Self-Lubricating Composites at a Wide Temperature Range

Penglin Zhang [1,2], Gaopan Zhao [1,3], Wenzhen Wang [3,*], Bin Wang [1,3], Peiying Shi [3], Gang Qi [2] and Gewen Yi [3]

[1] State Key Laboratory of Advanced Processing and Recycling of Nonferrous Metals, Lanzhou University of Technology, Lanzhou 730050, China; zhangpl@lut.edu.cn (P.Z.); Chinagpanzhao@sohu.com (G.Z.); 18119341658@163.com (B.W.)

[2] Department of Mechanical Engineering, The University of Memphis, Memphis, TN 38152-3180, USA; gangqi@memphis.edu

[3] State Key Laboratory of Solid Lubrication, Lanzhou Institute of Chemical Physics, Chinese Academy of Sciences, Lanzhou 730000, China; peiyingshi@126.com (P.S.); gwyi@licp.cas.cn (G.Y.)

* Correspondence: wzhwang@licp.cas.cn; Tel.: +86-931-4968-135

Received: 15 January 2020; Accepted: 14 February 2020; Published: 18 February 2020

Abstract: A Cr-free Ni-based self-lubricating composites with MoS_2 and Ag as lubricants were fabricated by the powder metallurgy method. The microstructures were examined. The mechanical properties and tribological behaviors of the composites were evaluated from room temperature to 800 °C. The fractography was observed and the fracture mechanisms were analyzed. The morphologies and the phase compositions of worn surfaces were determined and the wear mechanisms were elaborated. The results indicate that MoS_2 did not completely decompose after sintering, and the NiMoAl-MoS_2-Ag composite has the best tribological properties (0.22, 1.68×10^{-5}) at 800 °C. The main wear mechanisms are micro-ploughing and plastic deformation. The improvement of tribological properties was attributed to the formation of the lubricating film consisting of NiO, Mo oxides, various molybdates, and Ag particles. The reactions resulting in these compositions are proposed. The mechanical properties degrade with the rise of temperature and the addition of lubricants. Both NiMoAl and NiMoAlAg alloys exhibit micro-void accumulation fracture while the composites with MoS_2 reveal intergranular fracture.

Keywords: self-lubricating composites; mechanical properties; tribological properties; fracture mechanisms; wide temperature range

1. Introduction

Metal matrix composites (MMCs) have been widely used in many fields such as the automobile industry, the nuclear power industry, and the aerospace industry due to their excellent mechanical properties, wear resistance, and the small thermal expansion coefficient [1–3]. As the working temperature of advanced engines increases continuously, the parts need to endure the high temperature and large temperature variation (start-stop and run), and, at the same time, most machine parts need to work under complex stress for a long time. The strength and lubrication of moving parts have become a key factor affecting the reliability and life of the entire system. Therefore, the unification of mechanical and lubricating properties over a wide temperature range (RT~800 °C) will become an important trend for the development of bulk materials [4,5]. Nickel (Ni) has a series of advantages such as high strength, satisfactory oxidation, hot corrosion resistance, and good

microstructure stability. In addition, Ni can become a solid solution made of other metal elements and does not precipitate in a deleterious phase. Thus, Ni is an excellent matrix metal and has been widely applied in advanced engines. Introducing eligible solid lubricants into strengthened nickel-based alloys is an effective way to achieve the unification of high mechanical properties and good tribological behaviors, which has attracted the attention of researchers at home and abroad [6–13].

Graphite and molybdenum disulfide (MoS_2) are a common solid lubricant and have low shear strength due to the lamellar structure. However, they will oxidize or decompose and lose lubrication at temperatures about 400 °C [14]. Silver (Ag), which is a soft metal, has often been added into composites as a lubricant serving at medium and low temperatures due to its low shear strength and large diffusion coefficient during sliding [15]. Metal oxides, fluoride, and oxysalt are high temperature lubricants [16–18]. Molybdates have gained increasing attention due to the lower friction coefficients at high temperatures [16,19–21]. Adding low and high temperature lubricants to the metal matrix can achieve continuous lubrication in a wide temperature range, but may lead to a significant decline in the comprehensive mechanical properties of the composite. Thus, an alternative approach of taking advantage of the synergistic effect of the extrinsic low temperature lubricants and the in-situ formed high temperature lubricants generated by a tribo-chemical reaction was proposed [22,23]. For instance, Aouadi et al. [22] studied the tribological properties and mechanisms of $Mo_2N/MoS_2/Ag$ coatings and found that the coatings exhibited lower friction coefficients (0.1~0.4) and wear rate (10^{-5}~10^{-7} mm^3/Nm) from room temperature (RT) to 600 °C, which is due to the synergistic effects of Ag and lubricious silver molybdate phases during the wear test. The anti-friction mechanism of silver molybdate at high temperatures was attributed to the lamellar structure [24]. Furthermore, NiMoAl-Cr_2O_3-based composites containing MoS_2 and Ag were reported to show wear rates (10^{-5}~10^{-4} mm^3/Nm) and friction coefficients (0.18~0.77) from RT to 700 °C when tested against Inconel 718 using a pin-on-disk high temperature tribometer [23] and the in-situ-formed silver molybdate was responsible for the good tribological properties at 700 °C. However, the mechanical properties of these materials in a wide temperature range, especially the high temperature mechanical properties are seldom reported. Most of the strength-related studies of self-lubricating materials only focus on the strength at RT. For example, Xiong et al. [25] investigated the flexural strength and tensile strength of Ni-based composites at RT as well as Ding et al. [26] tested the tensile strength of the PM304 composite at RT. Yang et al. [27] investigated the tensile and compressive properties of NiCrMoAl alloys from RT to 1000 °C, but the study is preliminary and needs further work. Furthermore, the reports on the deformation and fracture mechanisms of lubricating materials are even fewer. Consequently, the mechanical properties, the deformation, and fracture mechanisms of composites at a wide temperature range are attractive to the authors.

Accordingly, in this paper, the Nickel-base composites with Ni as the matrix, Mo and Al as the strengthening elements, and Ag and MoS_2 as the lubricants were prepared by a powder metallurgy (P/M) method. Cr is an important strengthening element in Ni-base superalloys and composites. However, in this paper, the Cr was excluded deliberately due to the possible complexity induced by Cr_xS_y [28–30] on the studies of mechanical and tribological properties. The mechanical and tribological properties of the Cr-free Nickel-based composites from room temperature to 800 °C will be synthetically studied. The fractography of composites at different temperatures will be investigated to elucidate the deformation-fracture mechanisms. Meanwhile, the morphologies and compositions of worn surfaces will be analyzed to understand the wear mechanisms.

2. Materials and Methods

The Nickel-based composites containing different contents of lubricants (see Table 1) were prepared by a powder metallurgical method. The raw materials were commercial Ni powder (60 μm, 99.50% purity, Jinchang Changqing, Jinchang, China), MoS_2 powder (1.5 μm, 98.50% purity, Shanghai Shenyu, Shanghai, China), Mo powder (48 μm, 99.95% purity), Al powder (48 μm, 99.80% purity), and Ag powder (25 μm, 99.99% purity). The latter three powders were purchased from Beijing Xing Rong Yuan Technology Co., LTD. The proportionally weighed powders were first ball-milled in zirconia jars and balls (balls to powders ratio of 10:1) by a planetary ball mill machine (QM-3SP4,

Nanjing university instrument plant, China) with a rotational speed of 400 rpm for 20 h. Then the powders after being milled were loaded into graphite die and hot pressed at 1050 °C–1100 °C with holding time of 30 min~1 h under the pressure of 25 MPa in a vacuum hot press sintering furnace (ZT-45-20Y, Shanghai Chen Hua, China) with the dynamic vacuum of about 10^{-2} Pa. After cooling, the sintered bulks were machined into the desired samples, and the surfaces were polished with 800 meshes emery paper and ultrasonically cleaned with acetone for the following tests and analyses.

The densities of composites are measured by using the AccuPyc 1330 automatic true density analyzer (AccuPyc 1330, Micromeritics, Atlanta, GA, USA). The hardness tests of the samples were conducted using an MH-5-VM microhardness tester (Shanghai Hengyi Science and Technology Corporation, Shanghai, China) on polished surfaces. For each sample, at least 10 tests were made with a load of 3 N and a hold time of 5 s, and the average values are given in Table 1.

The tensile and compressive tests at different temperatures were conducted in Instron 5582 (Instron Corporation, Norwood, MA, USA) and MTS E45.105 universal testing machines (MTS Systems Corporation, Eden Prairie, MN, USA) under atmospheric conditions. The specimens for the tensile and compressive tests are thin slab with the gauge dimension of 20 mm × 4 mm × 2 mm and the cylinder with a size of Φ 6 mm × 9 mm, respectively. The relevant standards for tensile and compression tests were GB/T 228.1–2010, GB/T 228.2–2015, and GB/T 7314–2007. All mechanical tests were performed at least three times under the same conditions to ensure the repeatability of test results, and the average values were shown. Before the test, the surfaces of each sample were ground to 600 # emery paper and then ultrasonically cleaned with acetone.

The friction and wear tests were using a ball-on-disk high temperature tribometer (UMT-3, Bruker Corporation, Billerica, MA, USA) under a dry sliding condition in air. The rotating disk samples were the Ni-based composites with a size of Φ 24 mm × 3 mm. The mating balls are Al_2O_3 (HV 16.5 GPa) with a diameter of 10 mm. Tests were conducted under a normal load of 20 N, a rotational speed of 200 rpm, and a wear track radius of 5 mm. The test temperatures were chosen to be RT, 400 °C, and 800 °C with a sliding distance of 377 m and duration time of 60 min. Before the test, all the specimens were ultrasonically cleaned in acetone. The friction coefficients were continuously recorded by the computer's own software (UMT Test, Bruker Corporation, Billerica, MA, USA) during the test. The volume loss ΔV was obtained by the equation below.

$$\Delta V = 2\pi RS \quad (1)$$

where R was the radius in meter and S was the abrasion profile area. Then the wear rate ω was calculated by Equation (2) below.

$$\omega = \Delta V/N \times L \quad (2)$$

where ω was the wear rate (mm^3/Nm), ΔV was the volume loss (mm^3), N was the load (N), and L was the sliding distance (m). The Non-contact optical profilometer (MicroXAM-800, KLA-Tencor Corporation, Milpitas, CA, USA) was used. The surface profile information can be obtained by micro interferometry and the area S of the wear trace profile of the composite can be calculated by software (Origin v8.0773, OriginLab Corporation, Northampton, MA, USA) integration. All the tribological tests were carried out at least two times under the same conditions to ensure the repeatability of the results, and the average results were given.

The phase structures and compositions of the samples were determined by X-ray diffraction analysis (D8 Discover high resolution, Bruker, Billerica, MA, USA) with Cu-Ka radiation in the 2θ range of 10°–80°. The microstructures, fractography, and morphologies of the wear surface of the samples were examined by scanning electron microscopy (SEM, Apreo S, Thermo Fisher Scientific, Waltham, MA, USA) equipped with energy dispersive spectroscopy (EDS). The contrast of backscattered electron imaging (BEI) was caused by different atomic numbers, so backscattered electron imaging (BEI) are generally used to distinguish different phases. The phase composition of worn surfaces was further analyzed by Confocal Micro Raman spectrometer (LabRAM HR Evolution, HORIBA Scientific, Paris, France) with a laser wavelength of 532 nm. In the field of tribology, Raman spectroscopy can be used to analyse the phase structure of the local area of the wear surface, which

can better reflect the change of wear surface composition with temperature. This reveals the lubrication mechanism.

3. Results

3.1. Density, Hardness, and Microstructures of Ni-Based Composites

Table 1 lists the hardness and densities of the composites. It can be seen that, compared with the N alloy, adding MoS_2 alone (NM) decreases the hardness and density. Introducing Ag alone (NA) significantly reduces the hardness, but increases the density of the material, while additions of Ag and MoS_2 together (NMA) lower the density and hardness of the composites, and the density and hardness values of NMA are between that of NA and NM.

Figure 1 displays the X-ray diffraction (XRD) patterns of the mixed powders and sintered composites. The XRD results of mixed powders indicate that the peaks of Ni become weaker and broad after milling with the addition of Ag and MoS_2 because of the grains refinement and the internal stress of phases [31]. After hot press sintering, the peaks of Al_2O_3 appeared, and Mo diffraction peaks disappear while hinting the solid solution of Mo into the Ni-based solution. For the MoS_2-containing composites (NM and NMA), after hot pressing, the MoS_2 peaks can also be detected, which indicates that MoS_2 did not decompose completely. This is inconsistent with Li and Xiong's reports [25].

Table 1. Compositions of composites and resulting densities and hardness.

Composite	Composition (wt.%)					Density	Vickers Hardness
	Ni	Mo	Al	MoS_2	Ag	(g/cm³)	(HV)
N	balance	5	5	0	0	7.82	321.47 ± 10.66
NM(MoS_2)	balance	5	5	10	0	7.65	296.39 ± 11.10
NA(Ag)	balance	5	5	0	10	8.43	177.14 ± 4.32
NMA(Ag/MoS_2)	balance	5	5	10	10	7.74	214.66 ± 24.76

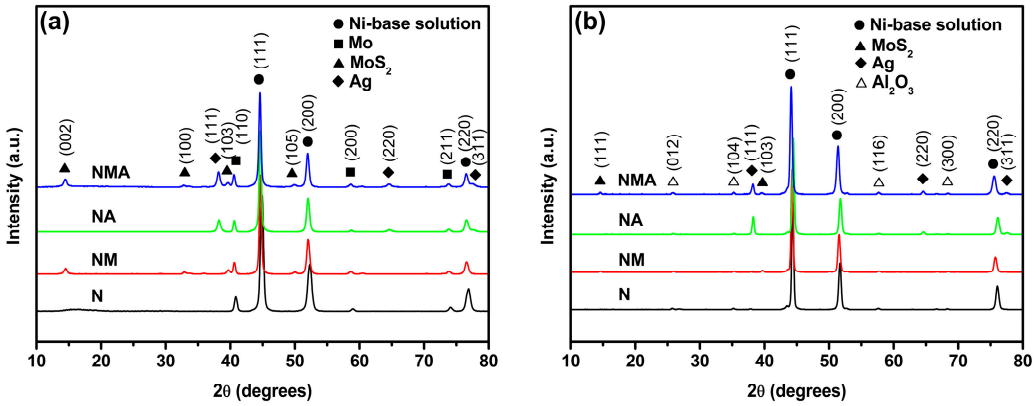

Figure 1. XRD patterns of the (**a**) mixed powders and (**b**) sintered composites.

Figure 2 shows the typical microstructures of the four Ni-based composites. For the N alloy, it contains a grey matrix phase and a dispersed deep grey phase. Combining the XRD and EDS results, we infer the grey matrix phase is Ni-based solution and the deep grey phase is Al_2O_3. For NM, the microstructures consist of grey Ni solution matrix phase, deep grey Al_2O_3, and flake-like white phases. The XRD and EDS exhibit the flake-like white phases are MoS_2. For NA, it includes Ni-solution, Al_2O_3, and continuous distributed Ag. For the NMA composite, it can be discovered that the microstructure is composed of four types of phases: the grey Ni matrix, deep grey Al_2O_3, flake-like MoS_2, and continuous Ag, respectively. The Ag and Al_2O_3 phases are well distributed in the matrix.

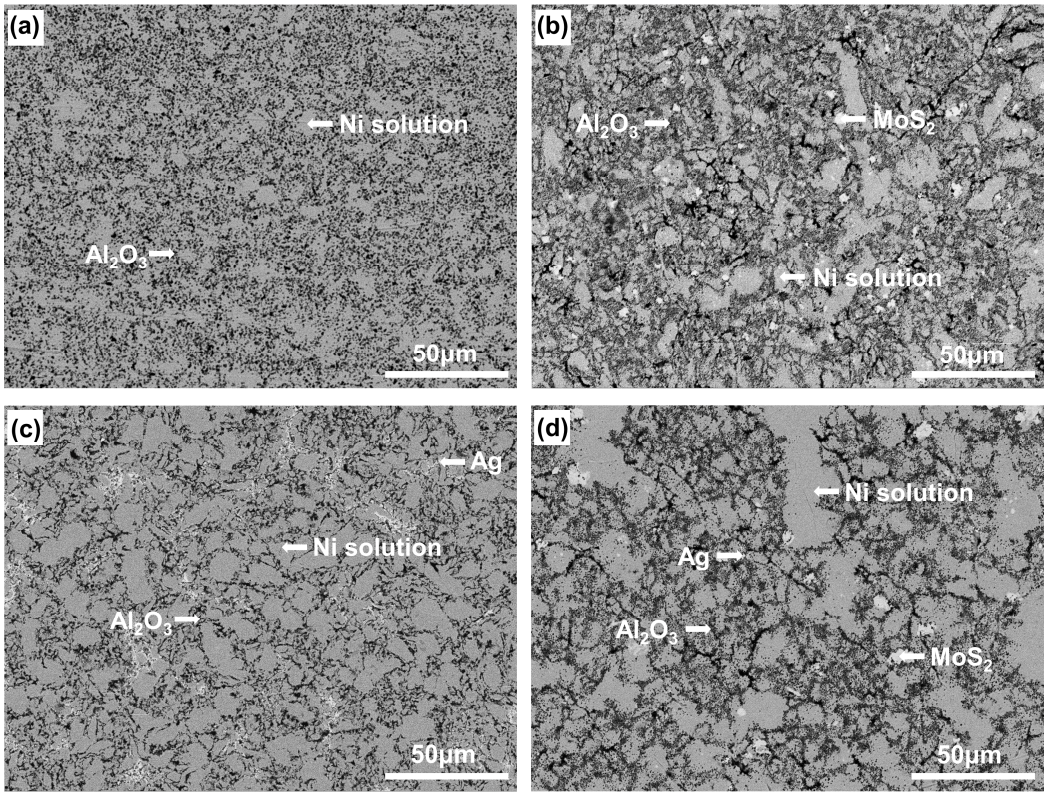

Figure 2. BEI micrographs of composites: (**a**) N, (**b**) NM, (**c**) NA, and (**d**) NMA.

3.2. Tribological Properties

Figure 3 shows the friction coefficients and wear rates of sintered Ni-based composites at different temperatures. It can be seen that, with the rise of temperature, the friction coefficients are lower generally, except the N and NA alloy. Both of them reveal the higher friction coefficients at 400 °C than at RT and 800 °C.

At RT, the wear rates of the four composites are favorable and on the order of 10^{-5}. While at 400 °C, the wear rates increase significantly and reach 2×10^{-4} mm³/Nm. When the temperature rises to 800 °C, the wear rates sharply drop to below 5×10^{-5} mm³/Nm. The N alloy has the lowest friction coefficient and wear rate at RT, while the NMA composite exhibits decent tribological properties at temperatures above 400 °C.

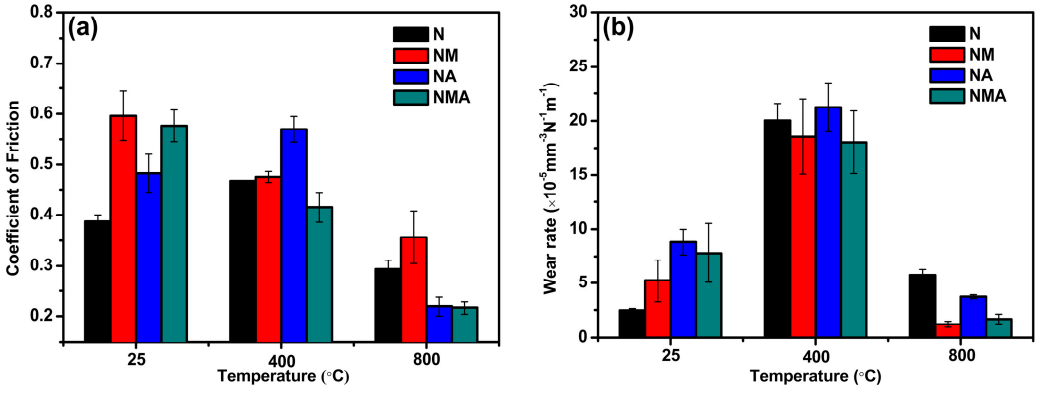

Figure 3. (**a**) Friction coefficients and (**b**) wear rates of Ni-based composites at different temperatures.

3.3. Mechanical Properties

The tensile and compressive strengths of the four composites at RT, 400 °C, and 800 °C are shown in Figure 4. With the increase of temperature, the strengths of the composites decrease, except for a slight increase in compressive strength of NM at 400 °C. Clearly, the Ni-based alloy without any lubricants has superior mechanical properties in the whole temperature range demonstrating that the lubricants decrease the mechanical strengths. Then, compared with other composites, the NA composite with Ag reveals relatively high mechanical properties in the range of RT~800 °C. The tensile and compressive strengths of the four composites at 1000 °C are also tested (not displayed in Figure 4), but the composites containing MoS_2 (NM and NMA) are so weak at this temperature that the strengths are negligible.

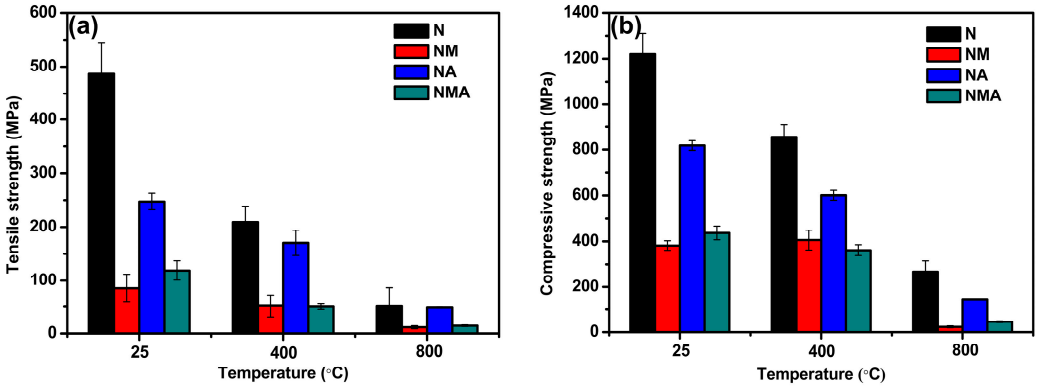

Figure 4. (**a**) Tensile strength and (**b**) compressive strength of Ni-based composites at different temperatures.

4. Discussion

4.1. Microstructures of the Composites

From the XRD patterns (Figure 1) and SEM micrographs (Figure 2), it can be observed that, after sintering, an appreciable MoS_2 phase still exists. Few of them decompose during sintering, which is somewhat surprising since, in the previous report, most MoS_2 decomposed during the sintering process and transformed into sulfide [28]. The main reason may be the absence of Cr in this study. In the previous study [32,33], the MoS_2 react with Cr as follows: $Cr + MoS_2 \rightarrow Cr_xS_{x+1} + Mo$ (x = 3,5) [25], and the element Cr acts as a "catalysis" and accelerate the decomposition of MoS_2. However, in this study, without the "catalysis", the sintering temperature of 1050–1100 °C is not high enough for the decomposition of MoS_2, which begins to decompose above 1370 °C.

4.2. Tribological Properties and Wear Mechanisms

The worn surface morphologies and the XRD patterns of the four composites after wear tests at different temperatures are displayed in Figures 5 and 6. At room temperature, for the N alloy, the shallow grooves and micro-cracks appear on the worn surface, and the main wear mechanism is micro cutting and micro-crack (Figure 5a$_1$). For NM, many spalling and delamination cover the worn surface (Figure 5b$_1$), and the wear mechanism is adhesive wear. For NA, grinding debris and spalling appear on the worn surface (Figure 5c$_1$), and the wear mechanism is dominated by abrasive wear. For NMA, the spalling and cracks of the worn surface can be clearly observed, and the wear mechanism is dominated by adhesive wear and a micro-crack (Figure 5d$_1$). The XRD patterns demonstrate no new phases emerge during the RT friction test. The tribological properties and wear mechanisms should be explained by the intrinsic microstructures of composites. For the N alloy, the micro-surface of the sintered material is relatively compact (Figure 2a) and results in slight wear, which corresponds to a lower friction coefficient and wear rate (Figure 3). For NM, it seems that the

remaining MoS_2 does not play the expected lubricating role, which can be explained that the MoS_2 particles are agglomerated and do not form a continuous lubricating film, and another explanation could be that the lubrication effect of MoS_2 is less than that of surface roughness caused by its addition. A similar explanation has been proposed by Ramalho [34]. For NA, the reason may be that the Ag phase distributed in the whole sample and, on the surface, it is not enough to form a continuous lubrication film. For NMA, the agglomerated MoS_2 and scattered Ag cannot provide the effective lubrication.

At 400 °C, for the N alloy, the worn surface of the former becomes rough and many spalling pits and delamination appear, and the wear mechanism is adhesive wear (Figure 5a$_2$). For NA, the wear scar is wide and deep on the worn surface and produces a lot of wear debris alongside the peeling pits, and the wear mechanism is dominated by abrasive wear (Figure 5c$_2$). For NM, the grooves with wear debris occur on the worn surface, which indicate the wear mechanism is dominated by abrasive wear (Figure 5b$_2$). For NMA, the grooves together with large pieces of spalling exist on the worn surface, and the wear mechanism is adhesive wear (Figure 5d$_2$). XRD patterns show the new oxides (NiO and MoO_2) appear. The sharp increase of wear rates at 400 °C is attributed to the decrease of hardness and the fragmentary oxides do not form continuous film but act as abrasives instead.

At 800 °C, for the N alloy, on the worn surface, there are large pieces of spalling pits and delamination, and the wear mechanism is mainly adhesive (Figure 5a$_3$). For NM, the worn surface appears as a relatively smooth film with some laminations, and the wear mechanism is mainly adhesive and plastic deformation (Figure 5b$_3$). For NA, the worn surface is relatively smooth, which is covered by a continuous glaze layer with some detachments. Thus, the main wear mechanism is plastic deformation (Figure 5c$_3$). For the NMA composite, the worn surface emerges a discontinuous glaze layer, and spalling and significant plastic deformation occur. The wear mechanism is mainly micro plow and plastic deformation (Figure 5d$_3$).

XRD patterns (Figure 6) display that for the N alloy except for the Ni-based solution and Al_2O_3, only the NiO can be detected, while, for NM, three new phases (MoO_2, MoO_3, $NiMoO_4$) appear. For NA, MoO_2, and Ag_2MoO_4 occur. For NMA, besides some oxides (NiO, MoO_2, MoO_3) and molybdates ($NiMoO_4$, Ag_2MoO_4), a new phase Ag_2O emerges. The metal oxides and molybdates are good high temperature lubricants, and the fewer lubricants in N alloy may explain the higher friction coefficient and wear rate at 800 °C. After an 800 °C friction test, the diffraction peaks of MoS_2 vanish, which means MoS_2 had oxidized. Previous studies [35,36] have reported that composite coatings containing MoS_2 and Ag required sulfur as a catalyst for the formation of silver molybdate. However, the results in this paper show that the S element is not necessary, and only Mo and Ag can also form silver molybdate at high temperatures, which is consistent with previous research results [23].

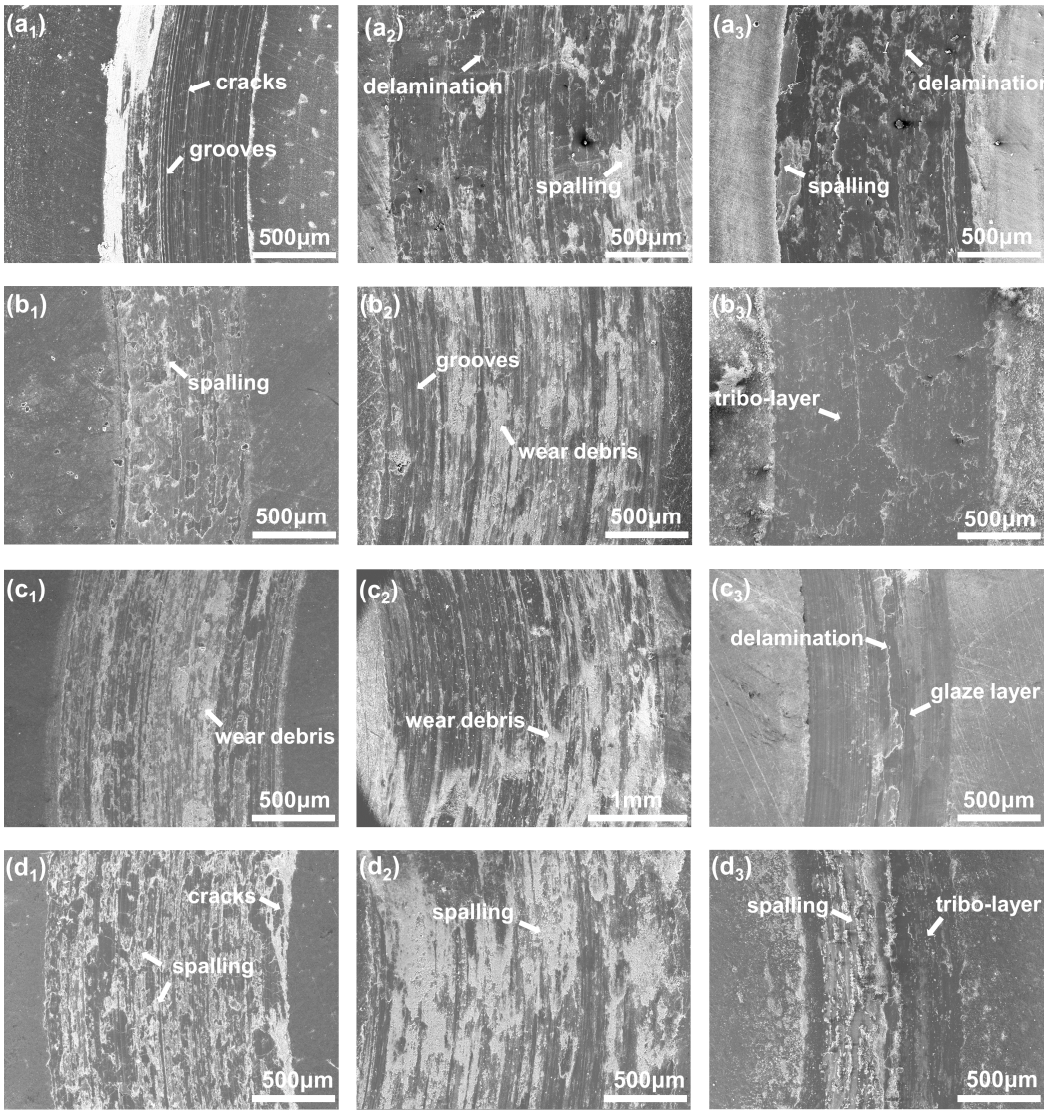

Figure 5. Worn surface SEM morphologies of (**a**) N, (**b**) NM, (**c**) NA, and (**d**) NMA composites tested at (**1**) RT, (**2**) 400 °C, and (**3**) 800 °C.

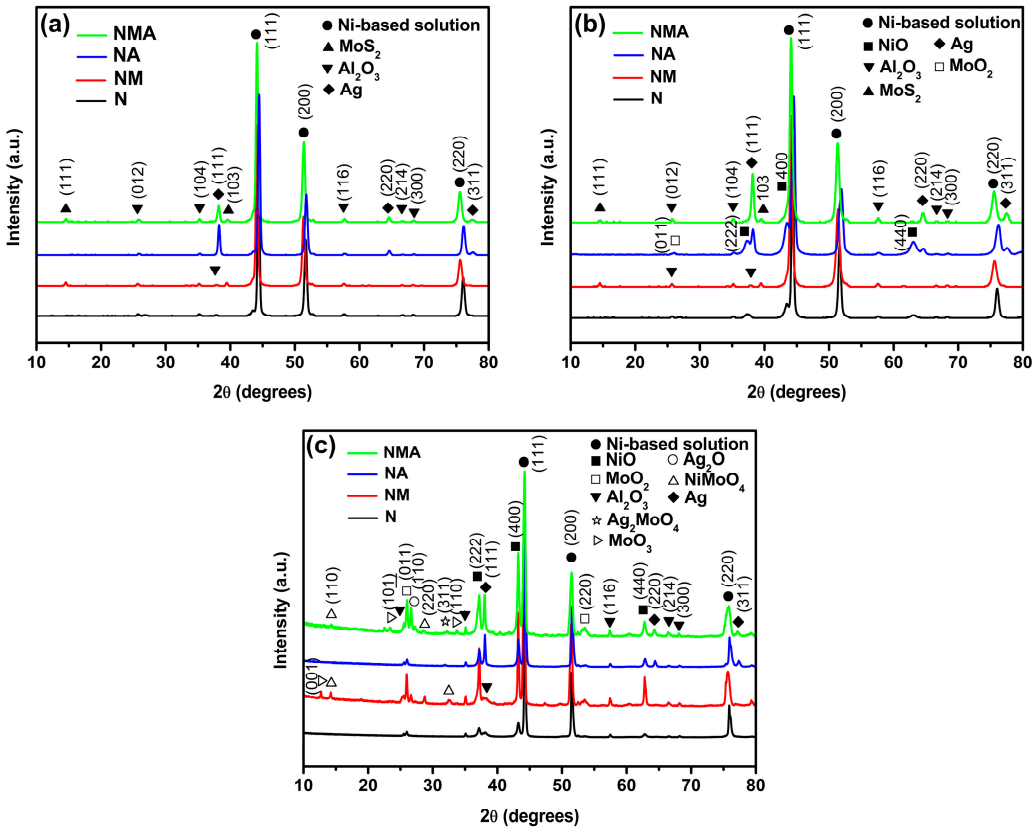

Figure 6. XRD patterns of the worn surface of a Ni-based composites test at (**a**) RT, (**b**) 400 °C, and (**c**) 800 °C.

In order to further analyze the compositions of the wear surface and explore the mechanisms of tribo-chemical reaction at 800 °C, the Raman analyses inside and outside the wear track were applied, and the results are given in Figure 7. For the N alloy, MoO_2 and NiO appear both inside and outside the wear track. The following reactions may occur.

$$2Ni+O_2 \rightarrow 2NiO \quad (3)$$

$$Mo+O_2 \rightarrow MoO_2 \quad (4)$$

For NM, outside the wear track, only NiO and MoO_2 can be detected, while, inside the wear track, NiO, MoO_2, MoO_3, and $NiMoO_4$ exist, which suggests the tribo-chemical reaction causes the formation of MoO_3 and $NiMoO_4$. It seems that, except reaction (3) and (4), the following reactions also occur.

$$2MoS_2+7O_2 \rightarrow 2MoO_3+4SO_2\uparrow \quad (5)$$

$$NiO+MoO_3 \rightarrow NiMoO_4 \quad (6)$$

For NA, Raman spectra reveal Ag_2MoO_4 only appear inside the wear track, which means it is generated by the tribo-chemical reaction. The most likely reactions are shown below.

$$4Ag+O_2 \rightarrow 2Ag_2O \quad (7)$$

$$Mo+O_2 \rightarrow MoO_2 \quad (8)$$

$$2MoO_2+O_2 \rightarrow 2MoO_3 \quad (9)$$

$$MoO_3+Ag_2O \rightarrow Ag_2MoO_4 \quad (10)$$

$$Mo+2Ag+2O_2 \rightarrow Ag_2MoO_4 \quad (11)$$

For NMA, besides the above-mentioned oxides and molybdates, a new molybdate $Ag_2Mo_2O_7$ appears, which can form by the following reactions.

$$2MoS_2+7O_2 \rightarrow 2MoO_3+4SO_2\uparrow \quad (12)$$

$$4Ag+O_2 \rightarrow 2Ag_2O \quad (13)$$

$$2MoO_3+Ag_2O \rightarrow Ag_2Mo_2O_7 \quad (14)$$

$$4Ag+2MoS_2+8O_2 \rightarrow Ag_2Mo_2O_7+Ag_2O+4SO_2\uparrow \quad (15)$$

NiO, MoO_3, and molybdates are easily deformed or sheared during high-temperature friction and, thus, have a low friction coefficient and wear rate [16,37]. The synergistic effects of NiO, MoO_2, MoO_3, $NiMoO_4$, Ag_2MoO_4, and $Ag_2Mo_2O_7$ are responsible for the excellent tribological properties of this composite.

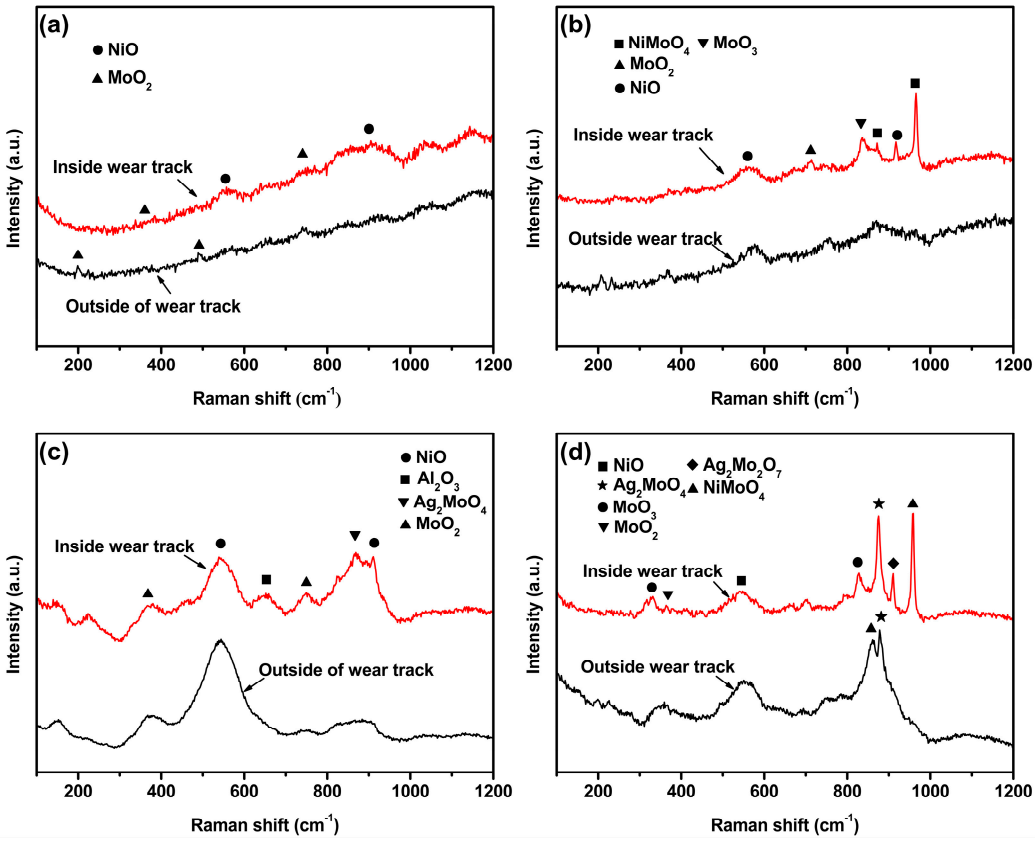

Figure 7. Raman spectra inside and outside the wear scar at 800 °C: (**a**) N, (**b**) NM, (**c**) NA, and (**d**) NMA composites.

Figures 8 and 9 shows SEM of the counter balls of N and NMA composites at different temperatures. It can be seen that they are similar with the wear trace of the disk sample. At RT, for the N alloy, relatively narrow material transfer widths indicate lower wear rates. For NMA, the material transfer is relatively wide and there are many substances, which indicates that the tribological properties are poor. At 400 °C, for N and NMA composites, material transfer increases and no continuous tribolayer is formed. At 800 °C, for the N alloy, on the transfer material, there are spalling pits and a thin tribolayer. For NMA, a continuous and thick tribolayer appears on the transfer material. Furthermore, the Raman and EDS analysis (Figure 10) of the transfer materials are present on the counter ball of NMA at 800 °C. The results show that the transferred material is mainly rich in Ni, Mo, Al, Ag, and O elements, which come from composites. Raman analysis shows the formation

of NiO and molybdate lubricant phases. The influence of the two composites on the counter balls is almost the same, which are both caused by the material transfer on the counter balls. Thus, this reduces the counter balls' wear. At high temperatures, the formation of a transfer film between the worn surfaces impede the direct contact of the friction pairs, which improves the tribological properties of the NMA composite and then avoids damage to the counter material.

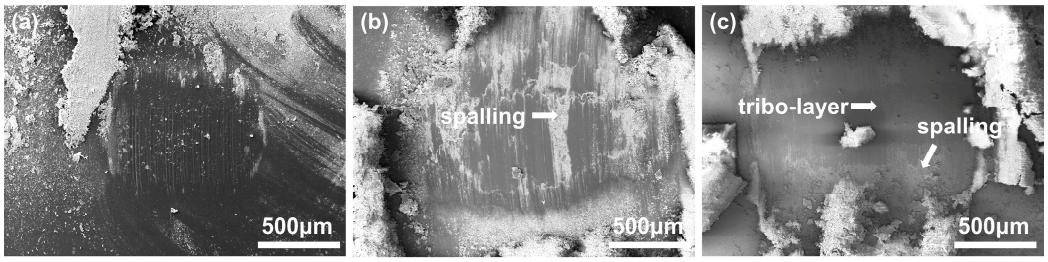

Figure 8. SEM of the Al_2O_3 counter ball, mating with N self-lubricating composite: (**a**) RT, (**b**) 400 °C, and (**c**) 800 °C.

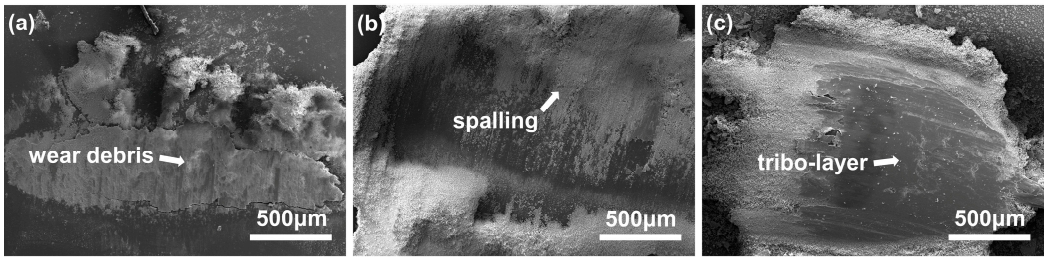

Figure 9. SEM of the Al_2O_3 counter ball, mating with NMA self-lubricating composite: (**a**) RT, (**b**) 400 °C, and (**c**) 800 °C.

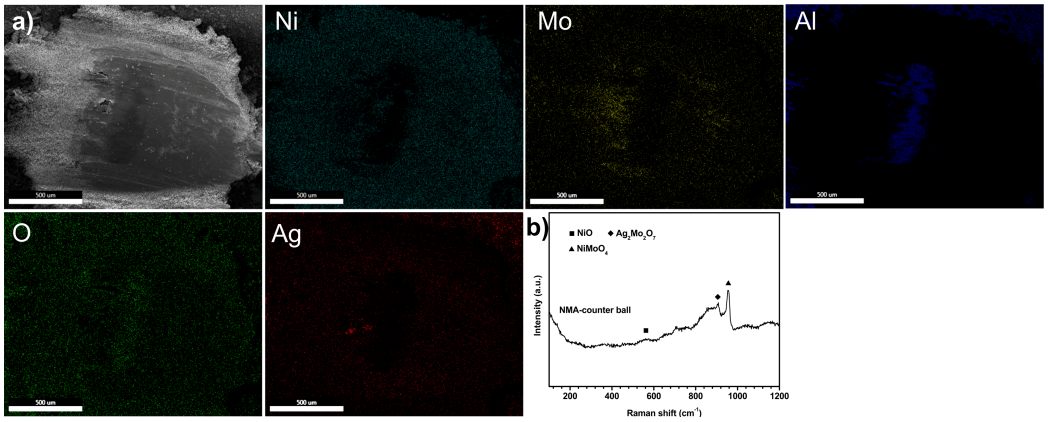

Figure 10. (**a**) EDS and (**b**) Raman spectra of the Al_2O_3 counter ball, mating with NMA self-lubricating a composite at 800 °C.

4.3. Mechanical Properties and Fracture Mechanisms

The fractography of N, NA, and NMA after different temperature tensile tests are indicated in Figure 11. For the N (NiMoAl) alloy, the fracture surfaces are characterized by a clear micro-void accumulation fracture (Figure 11a), which can be explained as follows. The sintered microstructures consist of fcc Ni-base solid solution and a few in-situ formed Al_2O_3 oxide. Under the tensile stress, first, the dislocations generate and glide in {111} face. Then, at the grain boundary or at the Ni/Al_2O_3 interface, the dislocations will pile up, and the continuous pile up give rise to the stress concentration.

When the stress concentration reaches a certain degree, the micropores could appear. Under the stress, these micropores would enlarge in size and the cracks may initiate and propagate at the micropores until the final rupture. The micro-void accumulation fracture is plastic fracture microscopically, but macroscopically, the NiMoAl alloy is brittle. For the NA alloy (NiMoAlAg), the fracture mechanisms are similar with that of N and reveal the micro-void accumulation fracture (Figure 11b). For the NM (not shown in Figure 11) and NMA composites (Figure 11c), the fracture surfaces are rather coarse and display the intergranular rupture.

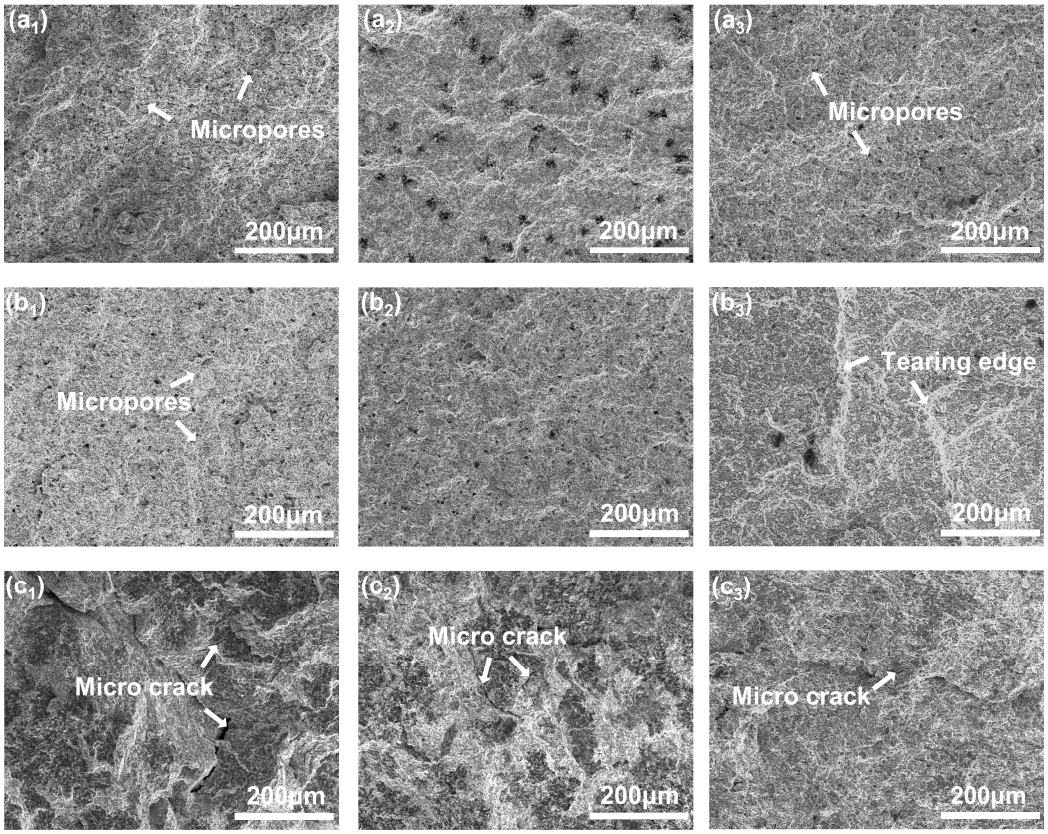

Figure 11. Fractography of (**a**) N, (**b**) NA, and (**c**) NMA composites after tensile test at (**1**) RT, (**2**) 400 °C, and (**3**) 800 °C.

The difference of strengths and fracture mechanisms should be attributed to the microstructure. For the N alloy, the microstructures consist of a Ni-base solid solution and in-situ formed Al_2O_3, and the refractory oxides segregate at the grain boundary and play the strengthening role in the alloy. Therefore, the strong grain boundaries impede the movement of dislocations and heighten the strength. For the NA alloy, because the solubility of Ag in Ni is very limited, the microstructures still contain silver aside from Ni-base solid solution and Al_2O_3 oxides. Due to the low melting point of Ag and the high fluidity at a high temperature, the Ag distributes uniformly in the matrix (Figure 2c). When the dislocations reach at Ag, it is easy for them to cut the soft Ag. Hence, the tensile and compressive strengths of NA are lower than those of N. Nevertheless, for the NM and NMA composite, the agglomerated molybdenum disulfide segregated at the grain boundary (Figure 2b,d), which weaken the grain boundary sharply and results in the intergranular fracture and the dramatical degradation of strength. The rise of test temperature did not change the fracture mechanism and the variation tendency of tensile and compressive strengths.

For now, in this study, it seems that it is difficult to achieve the unification of high mechanical properties and good continuous lubricating behaviors at a wide temperature range. The effect of mixed oxides on the mechanical properties of materials needs further study. Since MoS_2 is dramatically decreasing to the mechanical properties as well as its lubricating effect is not as

expected, we exclude MoS_2, and introduce another strengthening phase, such as tantalum (Ta) and dispersed strengthened Al_2O_3. The mechanical and tribological properties are investigated, and the results will be reported later.

5. Conclusions

In this paper, the mechanical and tribological properties and related mechanisms of Cr-free Ni-based self-lubricating composites with and without Ag/MoS_2 were studied from room temperature to 800 °C. The main conclusions can be drawn as follows.

(1) The addition of metal Ag decreased the hardness and increased the density, whereas the addition of MoS_2 has the opposite effect. In the MoS_2-containing composite, the sintered microstructures consist of appreciable undecomposed MoS_2, which means that the MoS_2 did not decompose completely.
(2) With the temperature rising, the friction coefficients of the composites reduce generally, and the wear rates increase abnormally at 400 °C, and then drop to lower than 5×10^{-5} mm^{-3}/Nm. The NiMoAl-MoS_2-Ag composite shows the best tribological properties at 800 °C (with a friction coefficient of 0.22 and a specific wear rate of 1.68×10^{-5} mm^{-3}/Nm), which was attributed to the formation of a lubricating film composed of NiO, Mo oxides, Ag_2O, various molybdates, and Ag particles at high temperature.
(3) With the addition of lubricants, the tensile and compressive strengths reduce. The NiMoAl and NiMoAlAg alloys exhibit micro void accumulation fracture, while the NiMoAl-MoS_2 and NiMoAl-Ag-MoS_2 composites reveal an intergranular fracture.

Author Contributions: Conceptualization, W.W. Methodology, experiments, formal analysis, G.Z., B.W., and P.S. Original draft, writing, G.Z. Review and editing, W.W. and G.Q. Resources, G.Y. Supervision, validation, project administration, P.Z. All authors have read and agreed to the published version of the manuscript.

Funding: The National Natural Science Foundation of China (Grant No. 51471181, 51575505, 51675508), Foundation of China Scholarship Council, and Achievements Transformation Foundation of Gansu Educational Committee (Grant No. 2017D-02) financially supported this work.

Conflicts of Interest: The authors declare no conflict of interest.

References

1. Dellacorte, C.; Sliney, H.E.; Bogdanski, M.S. Tribological and mechanical comparison of sintered and HIPped PM212: High temperature self-lubricating composites. *Lubr. Eng.* **1992**, *48*, 877–885.
2. Peng, W.X.; Sun, K.; Zhang, M.; Chen, J.; Shi, J.Q. Effects of deep cryogenic treatment on the microstructures and tribological properties of Iron matrix self-lubricating composites. *Metals* **2018**, *8*, 656, doi:10.3390/met8090656.
3. Hutchings, I.M. Tribological properties of metal matrix composites. *Mater. Sci. Technol.* **1994**, *10*, 513–517, doi:10.1179/mst.1994.10.6.513.
4. Zhu, S.Y.; Cheng, J.; Qiao, Z.H.; Yang, J. High temperature solid-lubricating materials: A review. *Tribol. Int.* **2019**, *133*, 206–223, doi:10.1016/j.triboint.2018.12.037.
5. Xue, Q.J.; Lu, J.J. The progress of high temperature solid lubricating materials. *Tribol. Int.* **1999**, *19*, 91–96, doi:10.3321/j.issn:1004-0595.1999.01.018.
6. Li, J.L.; Xiong, D.S.; Wu, H.Y.; Dai, J.H.; Cui, T. Tribological properties of molybdenized silver-containing nickel base alloy at elevated temperatures. *Tribol. Int.* **2009**, *42*, 1722–1729, doi:10.1016/j.triboint.2008.12.004.
7. Zhu, X.W.; Wei, X.F.; Huang, Y.X.; Wang, F.; Yan, P.P. High-temperature friction and wear properties of NiCr/hBN self-lubricating composites. *Metals* **2019**, *9*, 356, doi:10.3390/met9030356.
8. Wang, J.Y.; Shan, Y.; Guo, H.J.; Wang, W.Z.; Yi, G.W.; Jia, J.H. The tribological properties of NiCr–Al_2O_3–TiO_2 composites at elevated temperatures. *Tribol. Lett.* **2015**, *58*, doi:10.1007/s11249-015-0491-8.
9. Liu, E.Y.; Gao, Y.M.; Jia, J.H.; Bai, Y.P. Friction and wear behaviors of Ni-based composites containing Graphite/Ag_2MoO_4 lubricants. *Tribol. Lett.* **2013**, *50*, 313–322, doi:10.1007/s11249-013-0131-0.

10. Liu, F.; Yi, G.W.; Wang, W.Z.; Shan, Y.; Jia, J.H. Tribological properties of NiCr–Al_2O_3 cermet-based composites with addition of multiple-lubricants at elevated temperatures. *Tribol. Int.* **2013**, *67*, 164–173, doi:10.1016/j.triboint.2013.07.017.
11. Huang, C.B.; Du, L.Z.; Zhang, W.G. Preparation and characterization of atmospheric plasma-sprayed NiCr/Cr_3C_2–BaF_2·CaF_2 composite coating. *Surf. Coat. Technol.* **2009**, *203*, 3058–3065, doi:10.1016/j.surfcoat.2009.03.027.
12. Chen, J.; An, Y.; Yang, J.; Zhao, X.Q.; Yan, F.Y.; Zhou, H.D.; Chen, J.M. Tribological properties of adaptive NiCrAlY–Ag–Mo coatings prepared by atmospheric plasma spraying. *Surf. Coat. Technol.* **2013**, *235*, 521–528, doi:10.1016/j.surfcoat.2013.08.012.
13. Ding, C.H.; Li, P.L.; Ran, G.; Tian, Y.W.; Zhou, J.N. Tribological property of self-lubricating PM304 composite. *Wear* **2007**, *262*, 575–581, doi:10.1016/j.wear.2006.07.003.
14. Zabinski, J.S.; Donley, M.S.; Dyhouse, V.J.; McDevitt, N.T. Chemical and tribological characterization of PbO-MoS_2 films grown by pulsed laser deposition. *Thin Solid Films* **1992**, *214*, 156–163, doi:10.1016/0040-6090(92)90764-3.
15. Tyagi, R.; Xiong, D.S.; Li, J.; Dai, J. Elevated temperature tribological behavior of Ni based composites containing nano-silver and hBN. *Wear* **2010**, *269*, 884–890, doi:10.1016/j.wear.2010.08.022.
16. Petterson, M.B.; Calabrese, S.B.; Stupp, B. *Lubrication with Naturally Occurring Double Oxide Films*; Final Report; ONR Contract: Arlington, VA, USA, 1982. No. N0014-82-C-0247.
17. Kotkowiak, M.; Piasecki, A.; Kulka, M. The influence of solid lubricant on tribological properties of sintered Ni–20%CaF_2 composite material. *Ceram. Int.* **2019**, *45*, 17103–17113, doi: 10.1016/j.ceramint.2019.05.262.
18. Song, J.J.; Hu, L.T.; Qin, B.F.; Fan, H.Z.; Zhang, Y.S. Fabrication and tribological behavior of Al_2O_3/MoS_2–$BaSO_4$ laminated composites doped with in situ formed $BaMoO_4$. *Ceram. Int.* **2018**, *118*, 329–336, doi:10.1016/j.triboint.2017.09.032.
19. Chen, F.Y.; Feng, Y.; Shao, H.; Zhang, X.B.; Chen, J.; Chen, N.N. Friction and wear behaviors of Ag/MoS_2/G composite in different atmospheres and at different temperatures. *Tribol. Lett.* **2012**, *47*, 139–148, doi:10.1007/s11249-012-9970-3.
20. Liu, E.Y.; Gao, Y.M.; Wang, W.Z.; Zhang, X.L.; Wang, X.; Yi, G.W.; Jia, J.H. Effect of $Ag_2Mo_2O_7$ incorporation on the tribological characteristics of adaptive Ni-based composite at elevated temperatures. *Tribol. Trans.* **2013**, *56*, 469–479, doi:10.1080/10402004.2012.763004.
21. Wang, J.Y.; Shan, Y.; Guo, H.J.; Li, B.; Wang, W.Z.; Jia, J.H. Friction and wear characteristics of Hot-pressed NiCr–Mo/MoO_3/Ag self-lubrication composites at elevated temperatures up to 900 °C. *Tribol. Lett.* **2015**, *59*, doi:10.1007/s11249-015-0574-6.
22. Aouadi, S.M.; Paudel, Y.; Simonson, W.J.; Ge, Q.; Kohli, P.; Muratore, C.; Voevodin, A.A. Tribological investigation of adaptive Mo_2N/MoS_2/Ag coatings with high sulfur content. *Surf. Coat. Technol.* **2009**, *203*, 1304–1309, doi:10.1016/j.surfcoat.2008.10.040.
23. Liu, E.Y.; Wang, W.Z.; Gao, Y.M.; Jia, J.H. Tribological properties of Ni-based self-lubricating composites with addition of silver and molybdenum disulfide. *Tribol. Int.* **2013**, *57*, 235-241, doi:10.1016/j.triboint.2012.08.014.
24. Gulbiński, W.; Suszko, T. Thin films of Mo_2N/Ag nanocomposite—the structure, mechanical and tribological properties. *Surf. Coat. Technol.* **2006**, *201*, 1469–1476, doi:10.1016/j.surfcoat.2006.02.017.
25. Li, J.L.; Xiong, D.S.; Huo, M.F. Friction and wear properties of Ni–Cr–W–Al–Ti–MoS_2 at elevated temperatures and self-consumption phenomena. *Wear* **2008**, *265*, 566–575, doi:10.1016/j.wear.2007.11.024.
26. Ding, C.H.; Yang, Z.M.; Zhang, H.T.; Guo, Y.F.; Zhou, J.N. Microstructure and tensile strength of PM304 composite. *Composites Part A* **2007**, *38*, 348–352, doi:10.1016/j.compositesa.2006.03.011.
27. Yang, S.L.; Ma, Q.; Wang, W.Z.; Jia, J.H. Effect of molybdenum content on mechanical and tribological properties of nickel-base alloy. *Chin. J. Nonferrous Met.* **2017,** *27*, 2267–2275, doi:10.19476/j.ysxb.1004.0609.2017.11.11.
28. Li, J.L.; Xiong, D.S. Tribological properties of nickel-based self-lubricating composite at elevated temperature and counterface material selection. *Wear* **2008**, *265*, 533–539, doi:10.1016/j.wear.2007.09.005.
29. Xiong, D.S. Lubrication behavior of Ni-Cr-based alloys containing MoS_2 at high temperature. *Wear* **2001**, *251*, 1094-1099, doi:10.1016/S0043-1648(01)00803-1.
30. Liu, E.Y.; Gao, Y.M.; Wang, W.Z.; Zhang, X.L.; Wang, X.; Yi, G.W.; Jia, J.H. Effect of the synergetic action on tribological characteristics of Ni-based composites containing multiple-lubricants. *Tribol. Lett.* **2012**, *47*, 399–408, doi:10.1007/s11249-012-9991-y.

31. Ding, C.H.; Li, P.L.; Ran, G.; Zhou, J.N. PM304 coating on a Ni-based superalloy rod for high temperature lubrication. *Ceram. Int.* **2008**, *34*, 279–284, doi:10.1016/j.ceramint.2006.09.016.
32. Liu, R.T.; Li, X.B.; Cheng, S.H. Self-lubrication mechanism of Ni-Cr-Mo-S alloy. *Chin. J. Nonferrous Met.* **2003**, *13*, 469–473, doi:10.3321/j.issn:1004-0609.2003.02.037.
33. Xue, M.Q. High temperature oxidation and wear behaviour of powder metallurgically developed Ni-Cr-W-Al-Ti-MoS_2 composite. *Indian J. Eng. Mater. Sci.* **2009**, *16*, 111–115.
34. Ramalho, A.; Miranda, J.C. Friction and wear of electroless NiP and NiP+PTFE coatings. *Wear* **2005**, *259*, 828–834, doi:10.1016/j.wear.2005.02.052.
35. Muratore, C.; Voevodin, A.A. Molybdenum disulfide as a lubricant and catalyst in adaptive nanocomposite coatings. *Surf. Coat. Technol.* **2006**, *201*, 4125–4130, doi:10.1016/j.surfcoat.2006.08.014.
36. Aouadi, S.M.; Paudel, Y.; Luster, B.; Stadler, S.; Kohli, P.; Muratore, C.; Hager, C.; Voevodin, A.A. Adaptive Mo_2N/MoS_2/Ag tribological nanocomposite coatings for aerospace applications. *Tribol. Lett.* **2008**, *29*, 95–103, doi:10.1007/s11249-007-9286-x.
37. Li, B.; Jia, J.H.; Gao, Y.M.; Han, M.M.; Wang, W.Z. Microstructural and tribological characterization of NiAl matrix self-lubricating composite coatings by atmospheric plasma spraying. *Tribol. Int.* **2017**, *109*, 563–570, doi:10.1016/j.triboint.2017.01.031.